

RESEARCH

Open Access



Radiomic features from multiparametric magnetic resonance imaging predict molecular subgroups of pediatric low-grade gliomas

Zhen Liu^{1†}, Xuanke Hong^{1†}, Linglong Wang^{2†}, Zeyu Ma^{1†}, Fangzhan Guan¹, Weiwei Wang³, Yuning Qiu¹, Xueping Zhang⁴, Wenchao Duan¹, Minkai Wang¹, Chen Sun¹, Yuanshen Zhao^{5,6}, Jingxian Duan^{5,6}, Qiuchang Sun^{5,6}, Lin Liu⁷, Lei Ding⁷, Yuchen Ji¹, Dongming Yan¹, Xianzhi Liu¹, Jingliang Cheng⁴, Zhenyu Zhang^{1*}, Zhi-Cheng Li^{5,6,8*} and Jing Yan^{4*}

Abstract

Background We aimed to develop machine learning models for prediction of molecular subgroups (low-risk group and intermediate/high-risk group) and molecular marker (*KIAA1549-BRAF* fusion) of pediatric low-grade gliomas (PLGGs) based on radiomic features extracted from multiparametric MRI.

Methods 61 patients with PLGGs were included in this retrospective study, which were divided into a training set and an internal validation set at a ratio of 2:1 based on the molecular subgroups or the molecular marker. The patients were classified into low-risk and intermediate/high-risk groups, *BRAF* fusion positive and negative groups, respectively. We extracted 5929 radiomic features from multiparametric MRI. Thereafter, we removed redundant features, trained random forest models on the training set for predicting the molecular subgroups or the molecular marker, and validated their performance on the internal validation set. The performance of the prediction model was verified by 3-fold cross-validation.

Results We constructed the classification model differentiating low-risk PLGGs from intermediate/high-risk PLGGs using 4 relevant features, with an AUC of 0.833 and an accuracy of 76.2% in the internal validation set. In the prediction model for predicting *KIAA1549-BRAF* fusion using 4 relevant features, an AUC of 0.818 and an accuracy of 81.0% were achieved in the internal validation set.

[†]Zhen Liu, Xuanke Hong, Linglong Wang, and Zeyu Ma contributed equally to this work.

*Correspondence:
Zhenyu Zhang
fcczhangzy1@zzu.edu.cn
Zhi-Cheng Li
zc.li@siat.ac.cn
Jing Yan
fccyanj@zzu.edu.cn

Full list of author information is available at the end of the article



Conclusions The current study demonstrates that MRI radiomics is able to predict molecular subgroups of PLGGs and *KIAA1549-BRAF* fusion with satisfying sensitivity.

Trial registration This study was retrospectively registered at clinicaltrials.gov (NCT04217018).

Keywords Pediatric low-grade glioma, Magnetic resonance imaging, Radiomics, Machine learning, *BRAF* fusion

Background

Pediatric low-grade gliomas (PLGGs) are the most common pediatric brain tumors, accounting for more than 30% of central nervous system (CNS) tumors in children [1]. According to the 2016 World Health Organization (WHO) classification of CNS tumors, PLGGs comprise a histologically heterogeneous group of Grade I and II tumors, including pilocytic astrocytoma (PA, Grade I), diffuse astrocytoma (AII, Grade II), oligodendroglioma (OII, Grade II), oligoastrocytoma (OAI, Grade II), pleomorphic xanthoastrocytoma (PXA, Grade II), dysembryoplastic neuroepithelial tumor (Grade I), neuronal-glioma (Grades I and II) and several others [2]. In clinical practice, PLGGs are generally regarded as a single group of tumors with relatively quiescent biological behavior and favorable prognosis [1–3]. Nevertheless, recurrence or progression still occurs in about 30% of PLGGs [1, 2, 4]. Postoperative adjuvant therapies for PLGGs include radiation therapy and systematic chemotherapy, which may cause long-term morbidity and toxicity [1].

Compared to adult low-grade gliomas, PLGGs have different features in molecular pathology [2]. Most PLGGs possess alterations in RAS/MAPK pathway, in which *BRAF* is a vital component [2, 5, 6]. In our previous study using a large set of 289 PLGGs to investigate biomarkers of molecular pathology and their clinical significance, the *KIAA1549-BRAF* fusion, *MYB* amplification, *CDKN2A* deletion, *BRAF*^{V600E}, *H3F3A*, *TERT* promoter mutations, and *ATRX* loss were identified in PLGGs [2]. Emphatically, the combination of the previous molecular markers has successfully categorized PLGGs into four molecular risk groups (low-risk, intermediate-I, intermediate-II, and high-risk) with distinct survivals [2]. These findings highlight the importance of molecular stratification in evaluation and management of PLGGs.

Non-invasive prediction of molecular biomarkers or groups of gliomas is challenging [7]. Recent progress on artificial intelligence (AI) algorithms has considerably promoted automatically quantifying radiologic patterns, and several clinically relevant molecular biomarkers or groups have been identified by leveraging on AI algorithms in adult gliomas [8–11]. Recently, Wagner MW et al. developed and validated a radiomic signature that is predictive of the *BRAF* status of PLGGs [12]. However, there is a lack of study investigating the relationship between radiological features and risk groups of

PLGGs defined by multiple molecular markers utilizing AI algorithms.

In the current study, radiomic features from multiparametric MRI, including T1-weighted, T1-weighted gadolinium contrast-enhanced, T2-weighted, fluid attenuated inversion recovery, and apparent diffusion coefficient images (T1, T1c, T2, FLAIR, and ADC), were extracted from 61 PLGG patients to construct models for prediction of molecular subgroups (low-risk group and intermediate/high-risk group) and molecular marker (*KIAA1549-BRAF* fusion) by leveraging machine learning algorithms. We aim to demonstrate that MRI patterns are significantly associated with key molecular biomarker and are able to predict molecular subgroups of PLGGs.

Methods

Patient enrollment

This study was a part of the registered clinical trial “MR Based Prediction of Molecular Pathology in Glioma Using Artificial Intelligence” (ClinicalTrials.gov ID: NCT04217018). The overview of the radiomic pipeline is illustrated in Fig. 1. This retrospective study was approved by the Human Scientific Ethics Committee of the First Affiliated Hospital of Zhengzhou University (No. 2019-KY-176), and the requirement for written informed consent was waived. 102 pediatric patients (Age<18) were diagnosed to have harbored primary PLGGs at the First Affiliated Hospital of Zhengzhou University (FAHZZU) between January 2011 and December 2016. The inclusion criteria for this study were: (1) newly diagnosed histologically confirmed PLGGs; (2) pretreatment MR imaging including T1, T1c, T2, FLAIR, and ADC; (3) MR images with sufficient image quality. After the patient enrollment process (Fig. 2), 61 patients were included in this study.

MR imaging acquisition

All local MR images in FAHZZU were acquired on 1.5 T or 3.0 T clinical MR scanners, including Siemens, Philips, and GE Healthcare. The brain imaging protocol included the following sequences: (a) axial T1 before and after intravenous administration of a 0.1 mmol/kg dose of gadolinium-based contrast agent (T1c); (b) axial T2; (c) axial FLAIR; (d) diffusion-weighted imaging (DWI) and the corresponding ADC maps generated with the software incorporated into the MRI unit. Detailed information about the MR machines and imaging parameters are

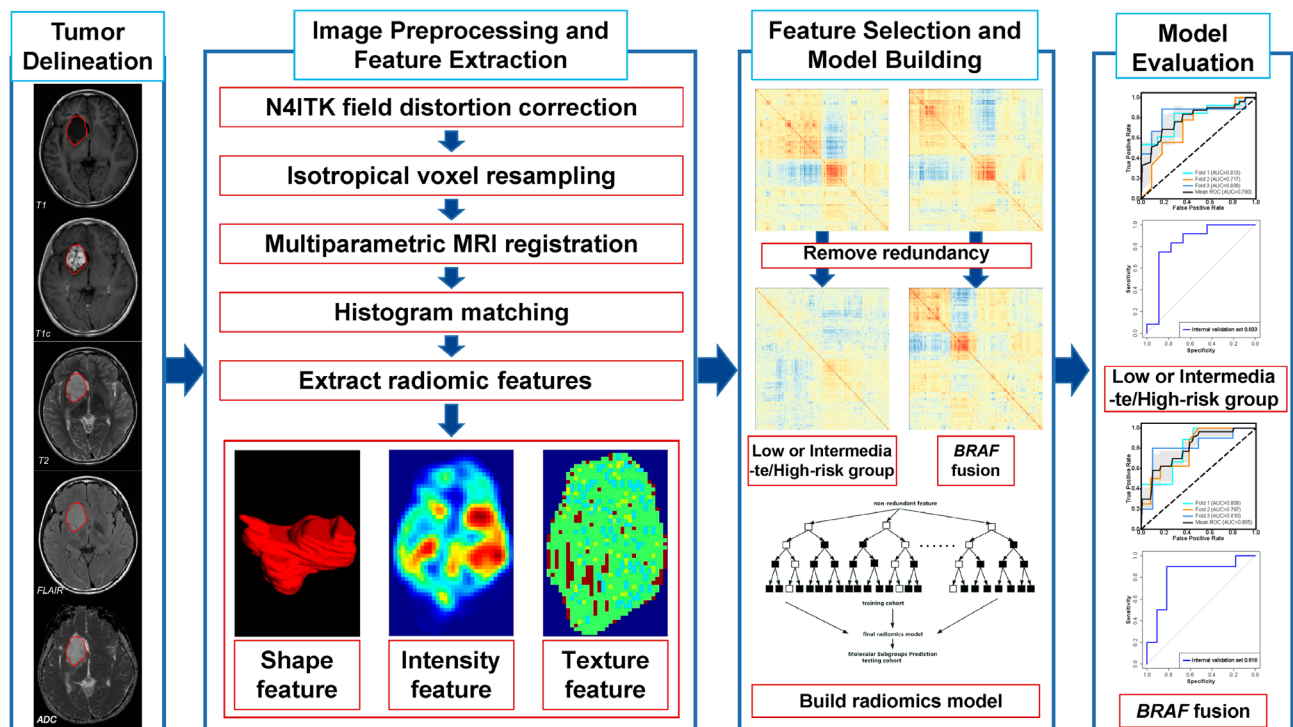


Fig. 1 Overview of the radiomic pipeline. The pipeline consisted of tumor delineation, image preprocessing, radiomic feature extraction, feature selection, model building, and model evaluation

available in Supplementary Material and Supplementary Table 1.

Detection of molecular pathology of PLGGs

Formalin-fixed paraffin embedded (FFPE) tissues were available in 102 cases. PCR and Sanger sequencing were performed to detect *TERT* promoter, *H3F3A*, *BRAF*, *FGFR1*, and *IDH1/2* mutations. *KIAA1549-BRAF* fusion, *MYB* amplification, and *CDKN2A* deletion were examined by Fluorescence in situ hybridization (FISH) analysis. Expression for ATRX and p53 proteins was evaluated by immunohistochemistry (IHC). Detailed protocols for the above molecular pathology were described by our previous research [2]. The molecular subgroups (low-risk and intermediate/high-risk) of PLGGs were assigned according to the integrative analysis of the above molecular markers [2]. Specifically, low-risk PLGGs were defined as patients with *BRAF* fusion or *MYB* amplification. Intermediate/high-risk PLGGs were defined as patients with *BRAF*^{V600E}, and/or *CDKN2A* deletion, or *TERT* mutation, or *H3F3A* mutation, or *ATRX* loss, or without alteration in any of the above biomarkers.

Image preprocessing and lesion segmentation

Image preprocessing pipeline was carried out to normalize the intensity and geometry using an open-source tool ITK (<https://itk.org/>). First, N4ITK-based bias field distortion correction was performed. Then, all voxels

were isotropically resampled into $1 \times 1 \times 1 \text{ mm}^3$ with trilinear interpolation. The multiparametric MR images were co-registered to the corresponding axial resampled T1c with mutual information similarity metric, generating the registered images rT1, rT1c, rT2, rFLAIR, and rADC. Histogram matching was performed to normalize the intensity distribution. The volumes of interest (VOIs) were drawn manually slice-by-slice via the ITK-SNAP software (www.itksnap.org) by an experienced radiologist (J.Y. with 11 years' experience) and consisted of the whole tumor regions (defined as the areas of abnormal signal on rFLAIR images). To assess the manual delineation-induced feature reproducibility, the VOI delineation process was repeated on 29 patients by another neurosurgeon (Z.Y.Z. with 11 years' experience).

High-throughput radiomic features extraction

All radiomic features were extracted using Pyradiomics extractor. To fully characterize the intra-tumor heterogeneity, three groups of features were extracted, including (1) shape features; (2) intensity features; and (3) texture features. Before feature extraction, fixed bin width of 25 was used for intensity discretization. The texture features were extracted using five different methods, including the gray-level co-occurrence matrix (GLCM), gray-level run length matrix (GLRLM), gray-level size zone matrix (GLSZM), gray-level dependence matrix (GLDM), and neighborhood gray-tone difference matrix (NGTDM).

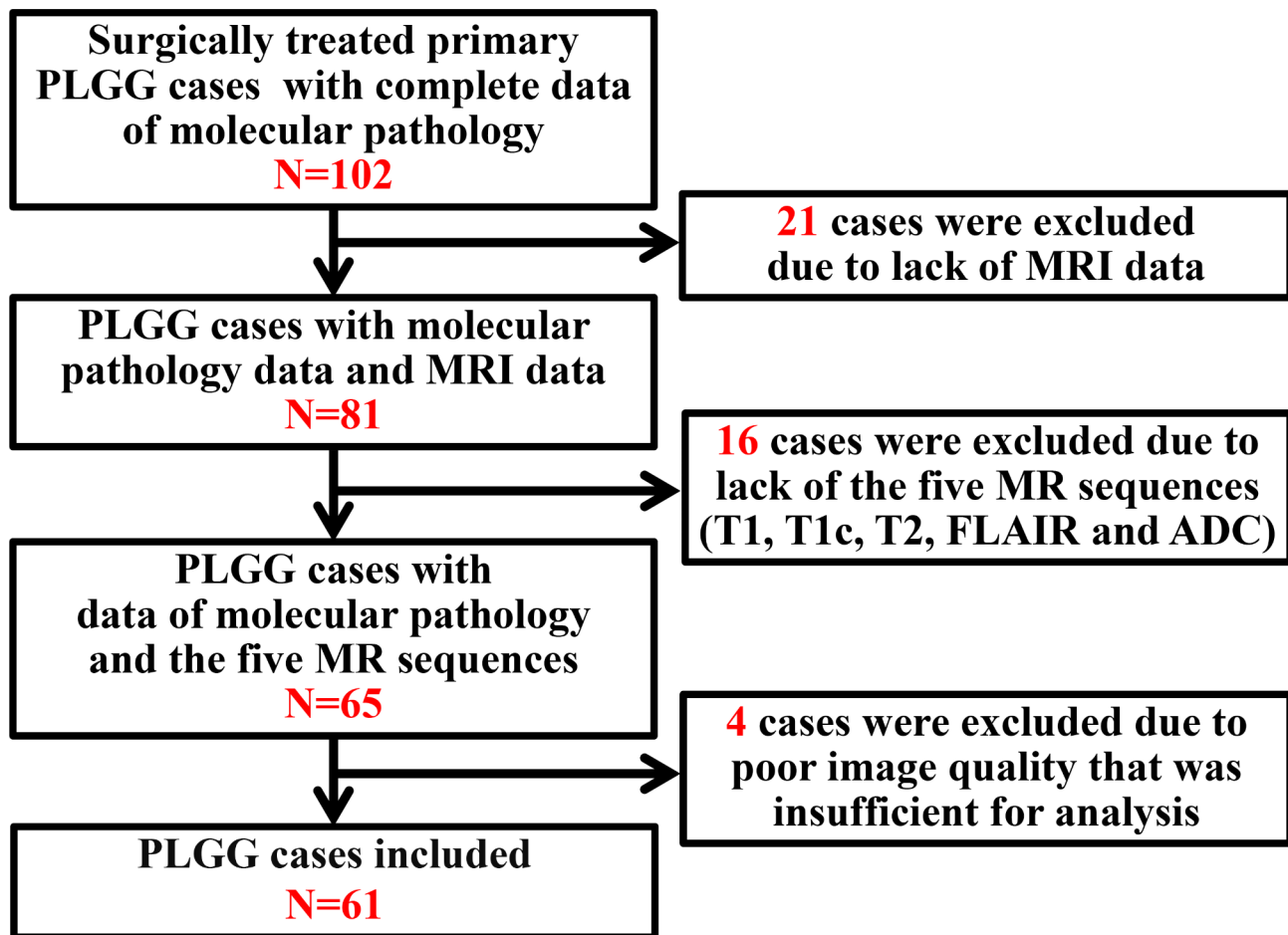


Fig. 2 The patient selection process in this study

Two filters [wavelet transform, Laplacian of Gaussian (LoG) with four sigma levels (2.0, 3.0, 4.0, and 5.0)] were enabled in extracting intensity features and texture features from both the original images and the transformed images. Finally, 5929 quantitative features (14 volume and shape features, 1170 intensity features, and 4745 texture features) were extracted from multiparametric MRI (rT1, rT1c, rT2, rFLAIR, and rADC) for each patient. The extracted features were summarized in Supplementary Table 2. The YAML file for feature extraction can be found in Supplementary Material.

Feature selection

Before feature selection, the stability of the extracted features was evaluated by interobserver reproducibility of the two image readers. We calculated the intraclass correlation coefficient (ICC) values between the same feature extracted from the two VOIs of 29 patients. The features with ICC value ≥ 0.90 were considered as highly reproducible features against the manual delineation and were retained for subsequent analysis while the others were discarded. Subsequently, all patients were randomly

divided into three equal sets to realize 3-fold cross-validation. Two of these sets were fixed as the training set and the other was fixed as the internal validation set, which was repeated three times. Once the sample was split, we applied z-score normalization to the features in the training set. Then, the feature distribution in the training set was used to normalize the features in the internal validation set.

Feature selection was performed for the training set in the following two steps. First, the correlation coefficients between each pair of the remaining features were calculated in their own training set to minimize the feature redundancy. For a feature pair with correlation coefficients greater than 0.75, the feature with better univariate predictive power (smaller Mann–Whitney U test P value) was retained, while the other was removed. Second, based on the remaining robust and non-redundant feature subset, a random forest-based wrapper feature selection algorithm Boruta [13] was used to further select the optimal and relevant features in training set. Boruta searched for relevant features iteratively by comparing the importance of original features with the importance

of artificially added random ones and progressively removing irrelevant features. After evaluating all possible feature combinations in the training set, the optimal features for the prediction model were selected.

Machine learning classification

Based on the selected features, the radiomic models were built using a random forest algorithm for predicting the molecular subgroups (low-risk group and intermediate/high-risk group) and molecular marker (*KIAA1549-BRAF* fusion), respectively. An R package caret was used for random forest model building. In the random forest algorithm, the decision tree was constructed adopting the classification and regression tree (CART) method to classify the molecular subgroups and molecular marker, where the Gini index was used as importance measure [14]. After assessing a set of numbers ranging from 50 to 800, the number of trees in the random forest algorithm

was set to 500. Here a 3-fold cross-validation was applied during model building. The data was partitioned into 3 folds, then 2 folds were used to train the model and the remaining fold was reserved for testing the model [15], and this process was repeated until the construction and evaluation of model was completed. Finally, the model of the best performance fold group of the 3-fold cross-validation scheme was chosen and validated.

Statistical analysis

The enrolled patients were randomly divided into a training set and an internal validation set at a ratio of 2:1, where the distribution of clinical information was balanced. The differences in sex, age, molecular subgroups, and molecular marker between the training and internal validation sets were assessed by using the Wilcoxon test or Chi-square test. The classification performance was assessed in terms of the area under the receiver operating characteristic (ROC) curve (AUC), accuracy (ACC), sensitivity (SEN), specificity (SPE), and precision. We repeated the model using 3-fold cross-validation to achieve the best diagnostic performance and determine the final predictive model. The statistical analysis employed R studio software (R-4.0.5).

Table 1 A summary of the clinical and molecular characteristics of patients (low-risk group and intermediate/high-risk group and *BRAF* fusion status) in PLGGs.

	Characteristic	Training set	Internal validation set	P Value
Risk group	Sex			0.33
	Male	20 (50.00%)	14 (66.67%)	
	Female	20 (50.00%)	7 (33.33%)	
	Age (year)			
	Mean ± SD	9.43 ± 4.93	9.81 ± 4.92	
	< 10	24 (60.00%)	11 (52.38%)	0.76
	≥ 10	16 (40.00%)	10 (47.62%)	
Risk group			1.00	
Intermediate/High	16 (40.00%)	9 (42.86%)		
Low	24 (60.00%)	12 (57.14%)		
<i>BRAF</i> fusion	Sex			0.08
	Male	26 (65.00%)	8 (38.10%)	
	Female	14 (35.00%)	13 (61.90%)	
	Age (year)			
	Mean ± SD	9.38 ± 5.11	9.90 ± 4.54	1.00
	< 10	23 (57.50%)	12 (57.14%)	
	≥ 10	17 (42.50%)	9 (42.86%)	
	<i>KIAA1549-BRAF</i> fusion			0.91
Yes	23 (57.50%)	11 (52.38%)		
No	17 (42.50%)	10 (47.62%)		

Results

Patient characteristics

Clinical and molecular characteristics of the 102 PLGGs surgically treated in FAHZZU were described in Supplementary Table 3. The models of optimal performance (risk group: fold 3; *BRAF* fusion: fold 3) in the cross-validation scheme were chosen. Patient characteristics of the training (n=40) and internal validation sets (n=21) were summarized in Table 1. There were no significant differences in the clinical and molecular characteristics between the training set and the internal validation set ($P=0.08-1.00$).

Feature selection

After the ICC repeatability test and Boruta algorithm, four all-relevant texture features were selected for the classification of molecular subgroups. Meanwhile, four all-relevant features were selected for the prediction of *BRAF* gene fusion, including three texture features and one intensity feature. The feature selection results were summarized in Table 2. To evaluate the univariate contribution of these features to the prediction of molecular subgroups and *BRAF* fusion, we calculated the Gini index as the importance value (Fig. 3). A larger value indicates greater importance in predicting a specific subgroup. In addition, the meanings of these selected features are described in Supplementary Table 4.

Table 2 A summary of the selected all-relevant features

	Selected features	Type	Sequence	Transform
Risk group	ClusterShade	texture	ADC	log. sigma.5.0.mm.3D
	DependenceEntropy	texture	ADC	wavelet.LLH
	DependenceEntropy	texture	FLAIR	log. sigma.2.0.mm.3D
	GrayLevelVariance	texture	T1	log. sigma.5.0.mm.3D
BRAF fusion	DependenceEntropy	texture	ADC	wavelet.LLH
	Minimum	intensity	T1c	original
	GrayLevelNonUniformity	texture	T1c	wavelet.LLL
	ClusterProminence	texture	T1	log. sigma.5.0.mm.3D

ADC: apparent diffusion coefficient; FLAIR: fluid attenuated inversion recovery; T1c: T1-weighted gadolinium contrast-enhanced; T1: T1-weighted

Prediction of molecular subgroups and BRAF fusion

The ROC curves with a 3-fold cross-validation scheme to predict molecular subgroups and BRAF fusion are shown in Fig. 4. By means of the optimal hyperparameters obtained from fold 3, the ROC curves of the two prediction models in both training and internal validation sets are calculated and displayed in Fig. 5. The performance of the prediction models is summarized in Table 3.

For the classification model of differentiating low-risk PLGGs from intermediate/high-risk PLGGs, the internal validation set yields an AUC of 0.833 (95% CI: 0.624-1.000). The ACC, SEN, SPE, and precision were 0.762 (95% CI: 0.550-0.900), 0.714 (95% CI: 0.571-0.905), 0.889 (95% CI: 0.667-1.000), and 0.900 (95% CI: 0.700-1.000), respectively.

For the prediction model of KIAA1549-BRAF fusion, the internal validation set yields an AUC of 0.818 (95% CI: 0.613-1.000). The ACC, SEN, SPE, and precision were

0.810 (95% CI: 0.666-0.952), 0.900 (95% CI: 0.700-1.000), 0.727 (95% CI: 0.455-1.000), and 0.750 (95% CI: 0.588-1.000), respectively.

Discussion

As the most frequent brain tumors in children, PLGGs comprise a group of gliomas with heterogeneous histological types and different tumor locations [16, 17]. In the past decades, novel biological insights into the genetic background of PLGGs have been acquired by extensive investigations [5, 6, 18-21]. Unlike adult low-grade gliomas that are characterized by robust molecular alterations such as IDH mutations, 1p/19q codeletion, and TERT promoter mutations [22-24], PLGGs harbor their own molecular alterations distinct from adult counterparts [3]. It was revealed that nearly all PLGGs converge on the alterations of the MAPK pathway, with these alterations 100% existing in pediatric pilocytic astrocytoma [5, 6]. The most common molecular alteration in the MAPK axis is KIAA1549-BRAF fusion, which is caused by tandem duplication and rearrangement between BRAF and KIAA1549 at chromosome 7q34 [2]. The BRAF gene is also the most common point mutation target in PLGGs, the majority being V600E hotspot mutation [19, 20]. Several studies have demonstrated that KIAA1549-BRAF fusion predicts better survivals in patients with PLGGs [2, 25], while BRAF^{V600E} point mutation is associated with inferior prognosis [26]. Aside from predictive values, BRAF gene alterations are also targets for novel drugs used in preliminary clinical trials for PLGGs. BRAF inhibitor such as dabrafenib has shown a positive response rate in a multicenter phase I study including patients with PLGGs [27]. Zhang J et al. reported 25% of diffuse cerebral gliomas in children carried abnormalities in MYB and MYBL1 using whole genome sequencing [6]. Our previous study has identified MYB amplification in 10.6% PLGGs and revealed this genetic alteration was



Fig. 3 The Gini index of the selected features

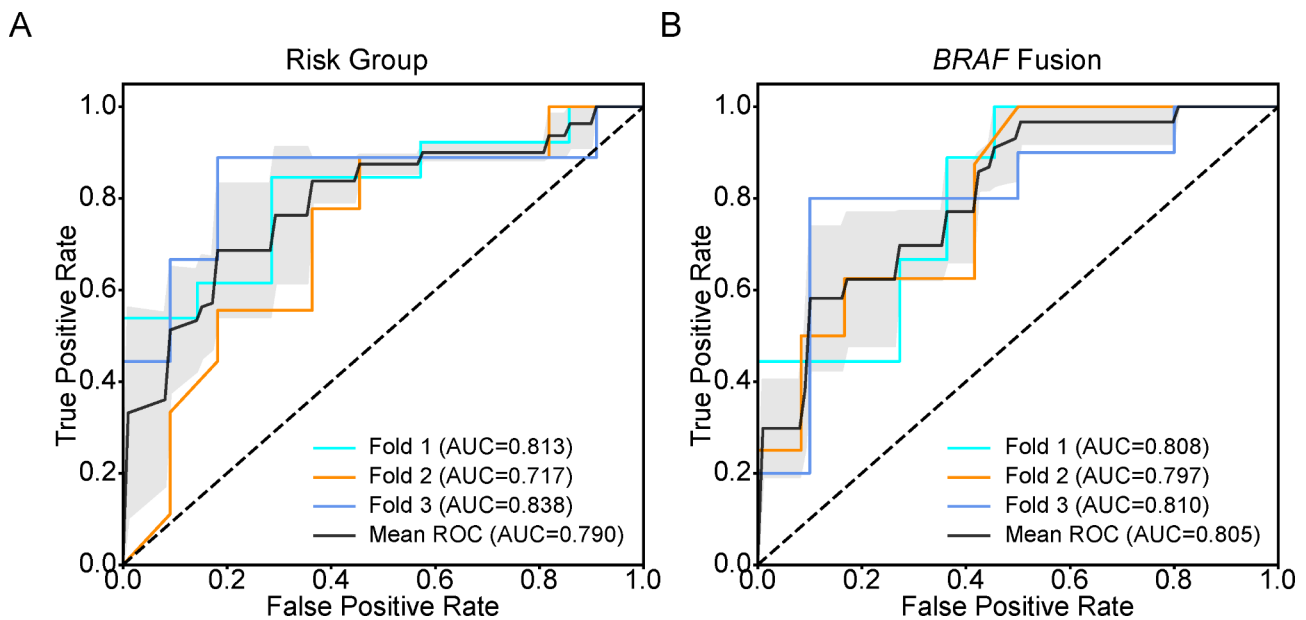


Fig. 4 The ROC curves of the radiomic models with a 3-fold cross-validation scheme for classification of low-risk group and intermediate/high-risk group (A), and prediction of *BRAF* fusion (B)

associated with significantly longer survivals of PLGGs. Therefore, the presence of either *KIAA1549-BRAF* fusion or *MYB* amplification categorizes a low-risk subset of PLGGs with a favorable prognosis [2].

Due to the limited number of intermediate ($n=23$) and high-risk ($n=2$) groups in the current set, we combined these two risk groups into one risk group (intermediate/high-risk group). Compared to the intermediate/high-risk group, the low-risk group of PLGGs confers an excellent survival with no mortality and rare tumor recurrence until the follow-up time point [2]. Therefore, identifying this group of PLGGs is of considerable significance since it has the potential to aid clinical decision-making such as the selection of molecular targeted therapies or curtailment of postoperative adjuvant therapies. However, the assignment of PLGGs risk groups requires the detection of multiple molecular biomarkers (*BRAF* fusion, *MYB* amplification, *BRAF*^{V600E} mutation, *CDKN2A* deletion, *TERT*_p mutation, *H3F3A* mutation, and *ATRX* loss), which are not all available in a vast number of medical centers with constrained resources. In addition, post-operative rather than the preoperative assignment of risk groups of PLGGs will inevitably lose the chance to guide personalized surgical resection strategies for these tumors. For instance, in low-risk group of PLGGs, it may be wise to perform palliative resection to preserve neurological function, rather than pursuing total tumor resection, since this group of PLGGs presents quiescent biological behavior.

Radiomics is an emerging research realm that investigates the relationship between radiographic features and tumor genotype, which serves as a promising approach

to discriminate surrogate biomarkers with an accurate reflection of tumor genomics [7]. Radiographic data from MRI of CNS tumors are also extensively investigated by radiomic strategies by leveraging AI algorithms, and adult gliomas are the most frequently studied CNS tumors [7]. Specifically, machine learning or deep learning algorithms trained on preoperative MRI were demonstrated to predict molecular biomarkers such as *IDH* mutations, 1p/19q codeletion, and *TERT* promoter mutations, or molecular subgroups based on *IDH* mutations and 1p/19q codeletion in adult gliomas with remarkable sensitivity and specificity [8–11]. A previous study has revealed radiomics-based prediction of *BRAF* status in PLGGs appears feasible [12]. However, whether radiomic features could accurately reflect the risk group of PLGGs remains unexplored. Our results demonstrated preoperative MRI patterns were able to predict either molecular biomarker (*BRAF* fusion) or risk group based on multiple molecular biomarkers, and yielded a satisfying performance, with AUC of 0.818 and 0.833, respectively.

It is worth noting that, identifying accurate and reproducible radiomic features of tumors is an essential step before translating into clinical application. As described in the previous literature, we employed a two-reader manual delineation approach by calculating the ICC between the same feature extracted from two VOIs to assess the feature reproducibility [28–30]. With the advancement of computing power, the use of semi-automatic or automatic approach has also provided sufficiently reliable tumor segmentation and feature stability [12, 31, 32].

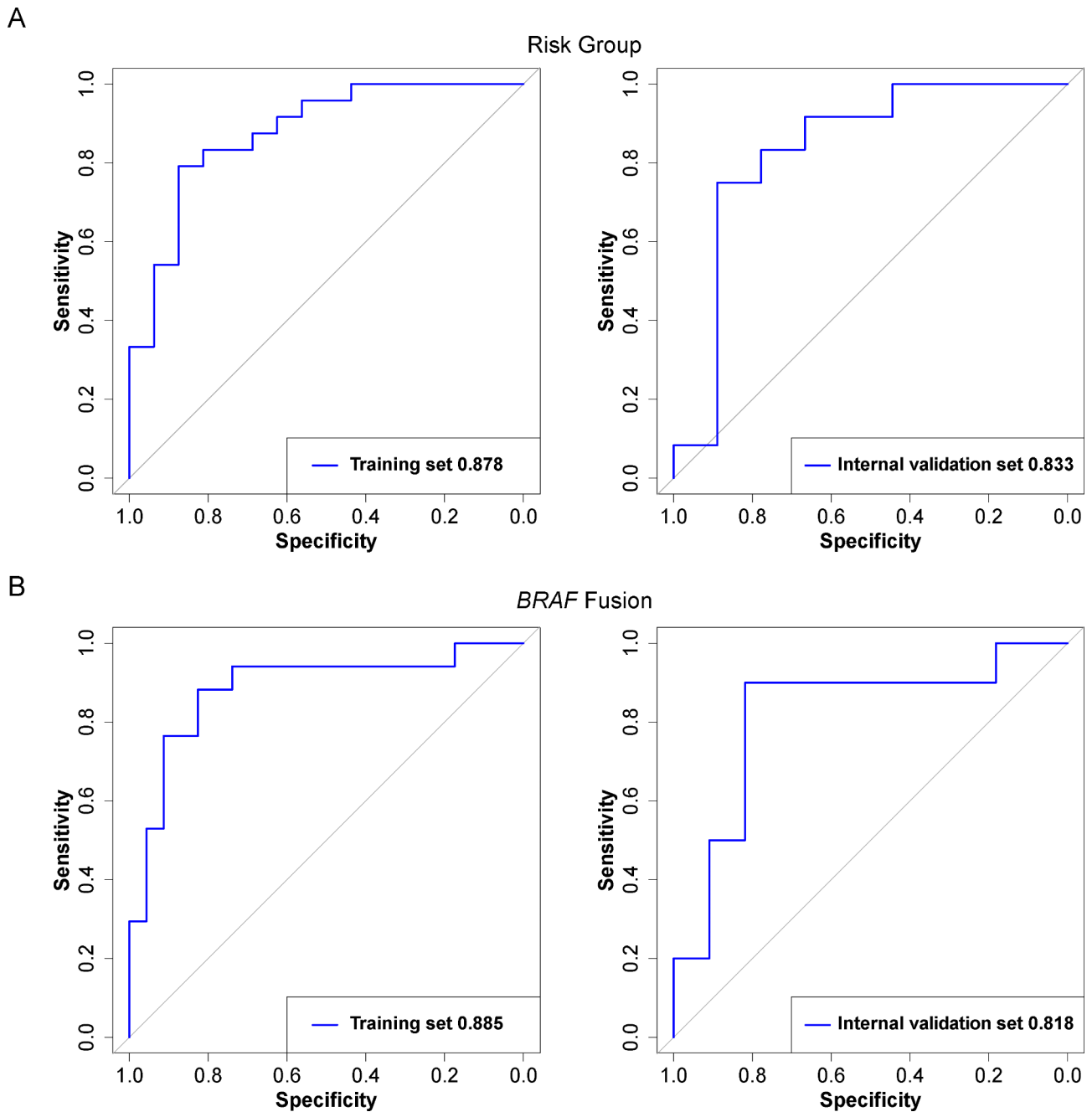


Fig. 5 The ROC curves in both training and internal validation sets using the optimal hyperparameters obtained by 3-fold cross-validation

Table 3 A summary of the subgroup-specific classification performance of the radiomic models

Molecular subgroups	Data Sets	AUC (95% CI)	ACC (%) (95% CI)	SEN (%) (95% CI)	SPE (%) (95% CI)	Precision (95% CI)
Low-risk vs. intermediate/high-risk	Training	0.878 (0.766, 0.989)	0.825 (0.700, 0.925)	0.792 (0.625, 0.917)	0.875 (0.688, 1.000)	0.909 (0.783, 1.000)
	Internal validation	0.833 (0.624, 1.000)	0.762 (0.550, 0.900)	0.714 (0.571, 0.905)	0.889 (0.667, 1.000)	0.900 (0.700, 1.000)
BRAF fusion positive vs. negative	Training	0.885 (0.770, 1.000)	0.850 (0.725, 0.950)	0.882 (0.706, 1.000)	0.826 (0.652, 0.957)	0.800 (0.650, 0.941)
	Internal validation	0.818 (0.613, 1.000)	0.810 (0.666, 0.952)	0.900 (0.700, 1.000)	0.727 (0.455, 1.000)	0.750 (0.588, 1.000)

AUC: area under the curve; ACC: accuracy; SEN: sensitivity; SPE: specificity; CI: confidence interval

To our knowledge, no prior study has investigated radiomic features of PLGGs using DWI. Our results indicate that the GLCM or GLDM texture features of ADC maps contribute to assess either molecular alteration or risk stratification in PLGGs. Likewise, it was reported that texture features and ADC parameters were important imaging markers to discriminate molecular subtypes in adult diffuse gliomas [9, 33–35]. For instance, Kihira S et al. found that addition of GLCM texture features from diffusion images to conventional MRI features could improve the diagnostic performance in determination of *MGMT* methylation status in gliomas [35]. Meanwhile, in our previous study, the results showed that the GLCM texture features from ADC maps played an important role in predicting *IDH* mutation and *TERT* promoter mutation of gliomas, while GLDM texture features from ADC maps were important for 1p/19q codeletion [9]. These phenomena may partly be explained by, that ADC values of brain tumors are inversely related to cellularity [36], and that texture features quantify local image patterns reflecting subtle intratumoral heterogeneity [33]. In addition, features from the conventional MR sequences were also revealed to play a role in the prediction model for *BRAF* status or risk stratification of PLGGs. This may explain why in the internal validation set, we archived a higher AUC (mean AUC=0.805) than the AUC (0.75) reported by the previous study using only FLAIR sequence for model development [12]. It is reasonable to infer that a radiomic signature with features from multiparametric MRI is more effective and reliable than a single sequence.

Several limitations need to be pointed out in the current study. The first limitation is the relatively small sample size of the set, which hampers us to divide the intermediate-risk group from high-risk group for developing prediction model. Multi-institutional studies with larger sample size are necessary to further validate our findings. Second, advanced MR sequences such as diffusion tensor imaging (DTI), perfusion-weighted imaging (PWI), and diffusion kurtosis imaging (DKI) are welcome to further excavate the potential of MRI for predicting genotypes of PLGGs. Third, extensive integrative analysis on high through-put sequencing with paired MRI data, as well as in vivo imaging studies are required to clarify the elusive mechanisms on the relationship between radiomic patterns and genotypes of PLGGs. Lastly, manual tumor segmentation is a time-consuming and costly task. In future, we will employ semi-automated or automated segmentation algorithms to achieve accurate and repeatable tumor segmentation.

Conclusions

Our findings suggest that radiomic patterns are significantly associated with molecular biomarker (*BRAF* fusion) and able to predict molecular subgroups of PLGGs with a satisfying performance. Investigations with larger sample size are welcomed to further unravel the relationship between radiomics and molecular biomarkers/subgroups of PLGGs.

Abbreviations

PLGG	Pediatric low-grade glioma
CNS	Central nervous system
WHO	World Health Organization
PA	Pilocytic astrocytoma
A	Astrocytoma
O	Oligodendroglioma
OA	Oligoastrocytoma
PXA	Pleomorphic xanthoastrocytoma
AI	Artificial intelligence
ADC	Apparent diffusion coefficient
DWI	Diffusion-weighted imaging
FFPE	Formalin-fixed paraffin embedded
FISH	Fluorescence in situ hybridization
IHC	Immunohistochemistry
GLCM	Gray-level co-occurrence matrix
GLRLM	Gray-level run length matrix
GLSZM	Gray-level size zone matrix
GLDM	Gray-level dependence matrix
NGTDM	Neighborhood gray-tone difference matrix
LoG	Laplacian of Gaussian
ROC	Receiver operating characteristic
AUC	Area under the curve
ACC	Accuracy
SEN	Sensitivity
SPE	Specificity
DTI	Diffusion tensor imaging
PWI	Perfusion-weighted imaging

Supplementary Information

The online version contains supplementary material available at <https://doi.org/10.1186/s12885-023-11338-8>.

Supplementary Material 1
 Supplementary Material 2
 Supplementary Material 3
 Supplementary Material 4
 Supplementary Material 5

Acknowledgements

The corresponding author acknowledges other authors for their contributions to this research.

Authors' contributions

JY, ZL, and ZZ were the main contributors to write the manuscript. XH, LW, FG, YZ, JD, ZM, and QS contributed in data analysis and interpretation. WW and YQ contributed in detection of molecular pathology of the disease. XZ, WD, MW, and CS contributed to data collection and image preprocessing. JY, ZL, ZZ, JC, XL, DY, ZM, and YJ contributed to study design, edited, and performed the final manuscript review. JY, LL, LD, ZL, ZZ, XL, WW, and YJ obtained fundings for the study. All authors read and approved the final manuscript.

Funding

This work was supported by the National Key R&D Program of China (grant number 2019YFC0117704), the National Natural Science Foundation of China

(grant numbers 82102149, 82273493, U20A20171, 61901458, 61571432, 81702465, 8217111948, U1804172, and U1904148), the Excellent Youth Talent Cultivation Program of Innovation in Health Science and Technology of Henan Province (grant number YXKC2022061), the Key Program of Medical Science and Technique Foundation of Henan Province (grant number SBGJ202002062), the Key-Area Research and Development Program of Guangdong Province (grant number 2021B0101420006), the Natural Science Foundation of Henan Province for Excellent Young Scholars (grant number 232300421057), and the Science and Technology Program of Henan Province (grant numbers 202102310136, 202102310138, 202102310113, and 202102310083).

Data Availability

All data generated or analyzed during this study are included in this published article.

Code Availability

The code scripts used in this article are deposited into github.com at <https://github.com/PLGG2023/Randomforest-code> and can be accessed and downloaded for free.

Declarations

Ethics approval and consent to participate

This retrospective study was approved by the Human Scientific Ethics Committee of the First Affiliated Hospital of Zhengzhou University (No. 2019-KY-176). The requirement for written informed consent was waived by the Human Scientific Ethics Committee of the First Affiliated Hospital of Zhengzhou University. All methods were carried out in accordance with relevant guidelines and regulations.

Consent for publication

Not applicable.

Competing interests

The authors declare that they have no competing interests.

Author details

¹Department of Neurosurgery, The First Affiliated Hospital of Zhengzhou University, Jian she Dong Road 1, Zhengzhou 450052, Henan province, China

²Yanjiang Medical College of Capital Medical University, Beijing, China

³Department of Pathology, The First Affiliated Hospital of Zhengzhou University, Zhengzhou, Henan, China

⁴Department of MRI, The First Affiliated Hospital of Zhengzhou University, Jian she Dong Road 1, Zhengzhou 450052, Henan province, China

⁵Institute of Biomedical and Health Engineering, Shenzhen Institute of Advanced Technology, Chinese Academy of Sciences, Shenzhen, China

⁶University of Chinese Academy of Sciences, Beijing, China

⁷China-Japan Union Hospital of Jilin University, Changchun, Jilin, China

⁸Shenzhen United Imaging Research Institute of Innovative Medical Equipment, Shenzhen 518045, China

Received: 25 October 2022 / Accepted: 25 August 2023

Published online: 11 September 2023

References

1. Raabe E, Kieran MW, Cohen KJ. New strategies in pediatric gliomas: molecular advances in pediatric low-grade gliomas as a model. *Clin Cancer Res*. 2013;19(17):4553–8.
2. Yang RR, Aibaidula A, Wang WW, Chan AK, Shi ZF, Zhang ZY, Chan DTM, Poon WS, Liu XZ, Li WC, et al. Pediatric low-grade gliomas can be molecularly stratified for risk. *Acta Neuropathol*. 2018;136(4):641–55.
3. Sturm D, Pfister SM, Jones DTW. Pediatric Gliomas: current concepts on diagnosis, Biology, and Clinical Management. *J Clin Oncol*. 2017;35(21):2370–7.
4. Wisoff JH, Sanford RA, Heier LA, Spoto R, Burger PC, Yates AJ, Holmes EJ, Kun LE. Primary neurosurgery for pediatric low-grade gliomas: a prospective multi-institutional study from the children's Oncology Group. *Neurosurgery*. 2011;68(6):1548–54. discussion 1554 – 1545.
5. Jones DT, Hutter B, Jäger N, Korshunov A, Kool M, Warnatz HJ, Zichner T, Lambert SR, Ryzhova M, Quang DA, et al. Recurrent somatic alterations of FGFR1 and NTRK2 in pilocytic astrocytoma. *Nat Genet*. 2013;45(8):927–32.
6. Zhang J, Wu G, Miller CP, Tatevossian RG, Dalton JD, Tang B, Orisme W, Punchihewa C, Parker M, Qaddoumi I, et al. Whole-genome sequencing identifies genetic alterations in pediatric low-grade gliomas. *Nat Genet*. 2013;45(6):602–12.
7. Bi WL, Hosny A, Schabath MB, Giger ML, Birkbak NJ, Mehrtash A, Allison T, Arnaout O, Abbosh C, Dunn IF, et al. Artificial intelligence in cancer imaging: clinical challenges and applications. *CA Cancer J Clin*. 2019;69(2):127–57.
8. Chang K, Bai HX, Zhou H, Su C, Bi WL, Agbodza E, Kavouridis VK, Senders JT, Boaro A, Beers A, et al. Residual convolutional neural network for the determination of IDH Status in Low- and High-Grade Gliomas from MR Imaging. *Clin Cancer Res*. 2018;24(5):1073–81.
9. Yan J, Zhang B, Zhang S, Cheng J, Liu X, Wang W, Dong Y, Zhang L, Mo X, Chen Q, et al. Quantitative MRI-based radiomics for noninvasively predicting molecular subtypes and survival in glioma patients. *NPJ Precis Oncol*. 2021;5(1):72.
10. Macyszyn L, Akbari H, Pisapia JM, Da X, Attiah M, Pigrish V, Bi Y, Pal S, Davuluri RV, Roccogrondi L, et al. Imaging patterns predict patient survival and molecular subtype in glioblastoma via machine learning techniques. *Neuro Oncol*. 2016;18(3):417–25.
11. Yan J, Zhang S, Sun Q, Wang W, Duan W, Wang L, Ding T, Pei D, Sun C, Wang W, et al. Predicting 1p/19q co-deletion status from magnetic resonance imaging using deep learning in adult-type diffuse lower-grade gliomas: a discovery and validation study. *Lab Invest*. 2022;102(2):154–9.
12. Wagner MW, Hainc N, Khalvati F, Namdar K, Figueiredo L, Sheng M, Laughlin S, Shroff MM, Bouffet E, Tabori U, et al. Radiomics of Pediatric Low-Grade Gliomas: toward a Pretherapeutic differentiation of BRAF-Mutated and BRAF-Fused tumors. *AJNR Am J Neuroradiol*. 2021;42(4):759–65.
13. Kursa MB, Rudnicki WR. Feature selection with the Boruta Package. *J Stat Softw*. 2010;36(11):1–13.
14. Breiman L. Random forests. *Mach Learn*. 2001;45(1):5–32.
15. Shur JD, Doran SJ, Kumar S, Ap Dafydd D, Downey K, O'Connor JPB, Papanikolaou N, Messiou C, Koh DM, Orton MR. Radiomics in Oncology: a practical guide. *Radiographics*. 2021;41(6):1717–32.
16. Ostrom QT, Gittleman H, Fulop J, Liu M, Blanda R, Kromer C, Wolinsky Y, Kruchko C, Barnholtz-Sloan JS. CBTRUS Statistical Report: primary brain and central nervous system tumors diagnosed in the United States in 2008–2012. *Neuro Oncol*. 2015;17(Suppl 4):iv1–iv62.
17. Sievert AJ, Fisher MJ. Pediatric low-grade gliomas.
18. Dahiya S, Haydon DH, Alvarado D, Gurnett CA, Gutmann DH, Leonard JR. BRAF(V600E) mutation is a negative prognosticator in pediatric ganglioglioma. *Acta Neuropathol*. 2013;125(6):901–10.
19. Dimitriadis E, Alexiou GA, Tsotsou P, Simeonidi E, Stefanaki K, Patereli A, Prodromou N, Pandis N. BRAF alterations in pediatric low grade gliomas and mixed neuronal-glioma tumors. *J Neurooncol*. 2013;113(3):353–8.
20. Dougherty MJ, Santi M, Brose MS, Ma C, Resnick AC, Sievert AJ, Storm PB, Biegel JA. Activating mutations in BRAF characterize a spectrum of pediatric low-grade gliomas. *Neuro Oncol*. 2010;12(7):621–30.
21. Tatevossian RG, Tang B, Dalton J, Forshew T, Lawson AR, Ma J, Neale G, Shurtleff SA, Bailey S, Gajjar A, et al. MYB upregulation and genetic aberrations in a subset of pediatric low-grade gliomas. *Acta Neuropathol*. 2010;120(6):731–43.
22. Yan H, Parsons DW, Jin G, McLendon R, Rasheed BA, Yuan W, Kos I, Batinic-Haberle I, Jones S, Riggins GJ, et al. IDH1 and IDH2 mutations in gliomas. *N Engl J Med*. 2009;360(8):765–73.
23. Smith JS, Perry A, Borell TJ, Lee HK, O'Fallon J, Hoseney SM, Kimmel D, Yates A, Burger PC, Scheithauer BW, et al. Alterations of chromosome arms 1p and 19q as predictors of survival in oligodendrogliomas, astrocytomas, and mixed oligoastrocytomas. *J Clin Oncol*. 2000;18(3):636–45.
24. Eckel-Passow JE, Lachance DH, Molinaro AM, Walsh KM, Decker PA, Sciotte H, Pekmezci M, Rice T, Kosel ML, Smirnov IV, et al. Glioma groups based on 1p/19q, IDH, and TERT promoter mutations in tumors. *N Engl J Med*. 2015;372(26):2499–508.
25. Johnson A, Severson E, Gay L, Vergilio JA, Elvin J, Suh J, Daniel S, Covert M, Frampton GM, Hsu S, et al. Comprehensive genomic profiling of 282 Pediatric Low- and High-Grade Gliomas reveals genomic drivers, Tumor Mutational Burden, and Hypermutation Signatures. *Oncologist*. 2017;22(12):1478–90.

26. Horbinski C, Nikiforova MN, Hagenkord JM, Hamilton RL, Pollack IF. Interplay among BRAF, p16, p53, and MIB1 in pediatric low-grade gliomas. *Neuro Oncol.* 2012;14(6):777–89.
27. Kieran MW. Targeting BRAF in pediatric brain tumors. *Am Soc Clin Oncol Educ Book* 2014:e436–440.
28. Aerts HJ, Velazquez ER, Leijenaar RT, Parmar C, Grossmann P, Carvalho S, Bussink J, Monshouwer R, Haibe-Kains B, Rietveld D, et al. Decoding tumour phenotype by noninvasive imaging using a quantitative radiomics approach. *Nat Commun.* 2014;5:4006.
29. Baeßler B, Weiss K, Pinto Dos Santos D. Robustness and reproducibility of Radiomics in magnetic resonance imaging: a Phantom Study. *Invest Radiol.* 2019;54(4):221–8.
30. Rizzetto F, Calderoni F, De Mattia C, Defeudis A, Giannini V, Mazzetti S, Vassallo L, Ghezzi S, Sartore-Bianchi A, Marsoni S, et al. Impact of inter-reader contouring variability on textural radiomics of colorectal liver metastases. *Eur Radiol Exp.* 2020;4(1):62.
31. Peng J, Kim DD, Patel JB, Zeng X, Huang J, Chang K, Xun X, Zhang C, Sollee J, Wu J, et al. Deep learning-based automatic tumor burden assessment of pediatric high-grade gliomas, medulloblastomas, and other leptomeningeal seeding tumors. *Neuro Oncol.* 2022;24(2):289–99.
32. Lee M, Woo B, Kuo MD, Jamshidi N, Kim JH. Quality of Radiomic features in Glioblastoma Multiforme: impact of semi-automated Tumor Segmentation Software. *Korean J Radiol.* 2017;18(3):498–509.
33. Lu CF, Hsu FT, Hsieh KL, Kao YJ, Cheng SJ, Hsu JB, Tsai PH, Chen RJ, Huang CC, Yen Y, et al. Machine learning-based Radiomics for Molecular Subtyping of Gliomas. *Clin Cancer Res.* 2018;24(18):4429–36.
34. Maynard J, Okuchi S, Wastling S, Busaidi AA, Almossawi O, Mbatha W, Brandner S, Jaunmuktane Z, Koc AM, Mancini L, et al. World Health Organization Grade II/III Glioma Molecular Status: prediction by MRI morphologic features and apparent diffusion coefficient. *Radiology.* 2021;298(1):E61.
35. Kihira S, Tsankova NM, Bauer A, Sakai Y, Mahmoudi K, Zubizarreta N, Houldsworth J, Khan F, Salamon N, Hormigo A, et al. Multiparametric MRI texture analysis in prediction of glioma biomarker status: added value of MR diffusion. *Neurooncol Adv.* 2021;3(1):vdab051.
36. Humphries PD, Sebire NJ, Siegel MJ, Olsen ØE. Tumors in pediatric patients at diffusion-weighted MR imaging: apparent diffusion coefficient and tumor cellularity. *Radiology.* 2007;245(3):848–54.

Publisher's Note

Springer Nature remains neutral with regard to jurisdictional claims in published maps and institutional affiliations.